

Your title  
in two rows  
or more

Master Thesis of

Your Name

At the Department of Physics  
Institut für experimentelle Teilchenphysik  
(ETP)

Reviewer: Prof. Dr. Wim de Boer  
Second reviewer: Prof. Dr. Second Advisor

Duration: 1. March 2017 – 28. February 2018



---

I declare that I have developed and written the enclosed thesis completely by myself, and have not used sources or means without declaration in the text.

**Karlsruhe, 24th January 2018**

.....  
**(Your Name)**



# Contents

<b>Introduction</b>	<b>1</b>
<b>1. Theory</b>	<b>3</b>
1.1. Our Milky Way . . . . .	3
1.1.1. General properties . . . . .	3
1.1.2. Dark Matter . . . . .	4
1.2. Physic of cosmic rays . . . . .	5
1.2.1. Creation of CR . . . . .	5
1.2.2. Propagation of CR . . . . .	5
1.2.3. Gamma-ray creation . . . . .	5
1.2.4. Gamma ray observation . . . . .	6
1.3. What are the unresolved problems of the precedent chapter . . . . .	6
<b>2. Method</b>	<b>9</b>
2.1. Data origin . . . . .	9
2.2. Model components . . . . .	11
2.2.1. Basic components . . . . .	11
2.2.2. Additional components . . . . .	12
2.3. Fitting method . . . . .	14
<b>3. Results</b>	<b>17</b>
3.1. Recreating previous results . . . . .	17
3.2. Introducing SCR . . . . .	17
3.3. Introducing SCR and MCR . . . . .	18
3.3.1. Discussion on spatial shapes . . . . .	19
3.4. Introducing SCR and DM . . . . .	21
3.5. Introducing SCR and MSP . . . . .	21
<b>4. Discussion</b>	<b>27</b>
4.1. Interpretation of spatial shapes . . . . .	27
4.2. Why is MCR better than DM or MSP . . . . .	27
4.3. How do these results fit in context . . . . .	27
<b>5. Conclusion</b>	<b>29</b>
<b>Bibliography</b>	<b>31</b>
<b>Appendix</b>	<b>35</b>
A. Some appendix section . . . . .	35



# **Introduction**

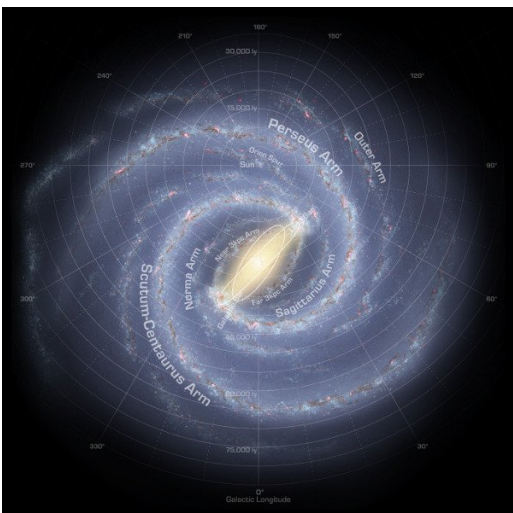
Awesome introduction.



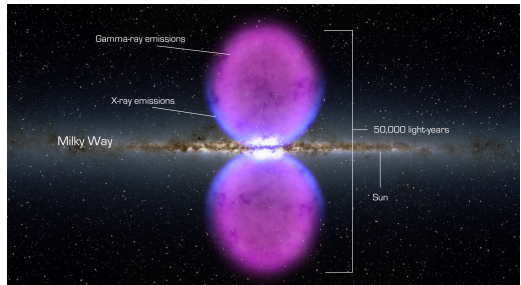
# 1. Theory

## 1.1. Our Milky Way

### 1.1.1. General properties



(a) source:  
<http://galaxymap.org/drupal/node/171>



(b) source: NASA's Goddard Space Flight Center

Figure 1.1.: The Milky Way, as seen from two different angles.

For a long time, people thought the universe was constituted only by one galaxy, the Milky Way, the one in which the Sun and the Earth orbit. The discoveries of other galaxies in the universe came only in the 20's thanks to Edwin Hubble. There is still a lot of unknown around those objects, but the Milky way is pretty well known and will play a major role in the following chapters. Its shape, density and composition are three main factors playing a role in cosmic ray physics and can not be avoided.

First of all, the Milky Way is a barred spiral arm galaxy, meaning it has two main spiral arms, connected in their center by a straight galactic bar. Those arms and bar have higher matter concentration than the rest due to the way stars orbit around the center.

Its diameter exceeds 40 kpc for a mass of around  $10^{12} M_{\odot}$  and a thickness under 1 kpc. The Sun and the Earth are rotating 8 kpc from its center in 240 Myr. All the different objects of the galaxy can be found in this thin disk of matter, mainly in the spiral arm. It includes the stars, planets and over massive objects, but also all the dust and gas clouds. As seen from the Earth, the disk looks like a narrow band of a few degrees in latitude, but with a very high concentration of gas and dust. In 2010, two large scale structures were detected to the north and the south of the GC. With a diameter of 7kpc, they extend up to 40 degrees in latitude and 20 in longitude. They are a source of high energy gamma-rays and were detected by the Fermi Large Area Telescope (LAT).

### 1.1.2. Dark Matter

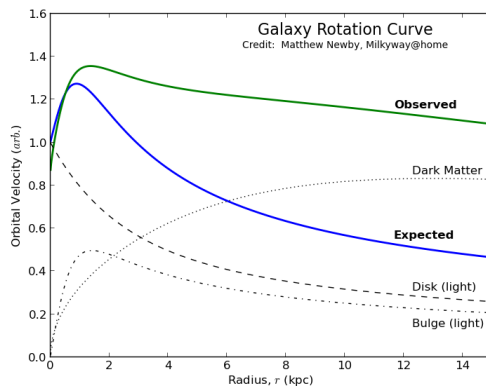


Figure 1.2.: Orbital velocity of the Milky Way as a function of the radius. A clear discrepancy between the theory and the observation can be seen above a 2 kpc radius. Source: Matthew Newby, Milkyway@home

The shape of spiral galaxies is well known today, with thousands of examples throughout the universe. This knowledge can be used to mathematically simulate them, and in particular their rotation time as a function of the distance to the center. It was a big surprise when the observed angular speed did not match the theory. One of the solution to explain this difference was the introduction in the standard model of the dark matter (DM), which was suppose to bring a lot of invisible mass into the system. It still has not been observed and a few theories exist on its exact nature. But even without knowing exactly what it is, its mass distribution can still be deduced from the observed rotation curve of the galaxy. The predicted distribution is a spherical halo extending way beyond the 40 kpc of the galactic matter disk. Its density peaks in the GC, and decrease with the radius following a particular density profile. The exact profile is not known, but a popular one is the Navarro-Frenk-White (NFW) profile defined as follows :

$$\rho(r) \propto \frac{1}{(r/r_S)(1+r/r_S)^2} \quad (1.1)$$

where  $r_S$  is the scale radius.

One of the most popular is the Weakly Interacting Massive Particles (WIMP). They are supposed to be non standard particles with a large mass, neutral, and only sensitive to the weak force, making them very difficult to observe.

## 1.2. Physic of cosmic rays

### 1.2.1. Creation of CR

### 1.2.2. Propagation of CR

Once they are emitted, the cosmic rays propagate through the galaxy under the influence of different interactions. The first one to notice is the complex manetic field created by all sorts of objects, from the stars to molecular clouds or any distribution of charged particles. It is not particularly strong (**put values**) compared to the heliosphere or what we can create on Earth, but its very large scale suffice to bend the CR's path in all direction until the point where it is impossible to backtrace its origin. An other possible interaction is the collisions with other particules. It will obviously depends on the density distribution of those colliders in the galaxy. We can expect a higher number of those in the disk, where the density of molecular clouds the highest.

**ToDo**

All these influences can be modeled by a diffusion model, mainly defined by its diffusion coefficient, which describes the average distance traveled in a certain time. The higher the coefficient, the faster a particule will diffuse in the galaxy. Each phenomenon can be attributed one of those coefficient to describe its effect on the cosmic rays. (**give values for Dmag, Dcoll...**) While the diffusion coefficient for the galactic magnetic field can be taken as constant throughout the milky way, the diffusion coefficient due to collision is proportional to the particles density. We can then expect a smaller coefficient in molecular clouds, where the density can reach (**value!**).

**ToDo**

**ToDo**

This coefficient will also define the cosmic ray densities in various locations of the galaxy. Indeed, the more a particle's path is twisted and convoluted, the harder it will be to escape move away from its origin. This way, a higher density of cosmic rays can be found in low diffusion coefficient areas like molecular clouds. In comparison, the region outside the galactic disk has a low density of CR due to a weak magnetic field and small gas and dust density. However, the bubble region is outside the disk and has a higher concentration of CR other regions outside the disk. This is due to a direct outward emission of CR from the GC region in the disk. With a high diffusion coefficient, those CR are ejected light years away (**put values**), forming two symetric region extending north and south up to 40 degrees in latitude.

**ToDo**

### 1.2.3. Gamma-ray creation

Since the cosmic rays we observe on Earth can not give us a clue about their origin, some indirect detection methods are requiered. Luckily, cosmic rays interact n a lot of ways with their environment, as discribed in the previous section. These interactions can leave detectable traces that can be observed. The most common is the production of light, via creation of high energy photon in the GeV range. Once created, these gamma rays can be blocked or absorbed, but not deflected. Linking the gamma-ray and cosmic ray requires to know the processes in play. Her eis a list of the main phenomena.

#### 1.2.3.1. Pion decay

The high energy protons can produce  $\pi^0$  which decay almost immediatly in 2 gammas of equal energy.

### 1.2.3.2. Bremsstrahlung

The electrons passing near an other charged particle, or in a magnetic field will be deflected by the electromagnetic interaction. In the process, the electron will lose energy via the emmision of photons. The energy of the latter will depend on the energy of the electron and the intensit of the magnetic ield or the charge of the other particule. The more the electron is deflected, the higher the energy of the emmited photons. (give numbers for B field and proton in MC)

ToDo

### 1.2.3.3. Inverse Compton

A third interaction can link the cosmic ray electrons to gamma rays and it is inverse compton. When a high energy electron collides with a low energy photons, the electron can transfert some of its kinetic energy to the photon, giving him enough energy to enter the gamma range.

So number of gamma rays coming from inverse compton is directly linked tto the electron distribution and the interstellar radiation field (ISRF) of the galaxy. The latter is composed of three major components, the starlight, the dust emission and the cosmological microwave background (CMB). The first component is directly linked to the star distribution, and will be dominant in the disk, where all the star are concentrated. The starlight emits as a blackbody, peaking in the UV range. The dust emission comes from the infra-red emission of warm dust. It will also be mainly present in the disk, since the dust clouds are pretty flat. Finally, the CMB is peaking in the microwave range but is unformely present everywhere in the universe, and therefor in the galaxy. It will be dominant where the two others are negligable, namely outside the galactic disk.

ToDo

(talk about synchrotron and ionization losses)

### 1.2.4. Gamma ray observation

Several instruments in the world observe gamma rays. For example the Fermi Large Area Telescope (LAT) mounted on the ISS. This instrument maps the gamma ray sky between 20MeV and 300GeV (cite). The diffuse cosmic ray emmision that we are interested in can be obtained after modeling and subtracting the contribution of the over sources. This allows us to compare the observation with the models we obtain from the previous three interactions.

ToDo

## 1.3. What are the unresolved problems of the precedent chapter

Several studies have already tried to see how our predictions of the gamma rays emis-  
sion and our observations compare. The three main phenomena were modeled as explained to try to recreate the spectrum observed from Earth. The results are clear, there are somethings missing in our interpretation. The fit is clearly not working in the galactic plane and the bubbles (as shown on Fig. 1.4. The spatial templates used in those fits also show a spherical excess of gamma rays of about 2GeV in the galactic center (GC).

Two main ideas have emerged to explain this spherical excess.

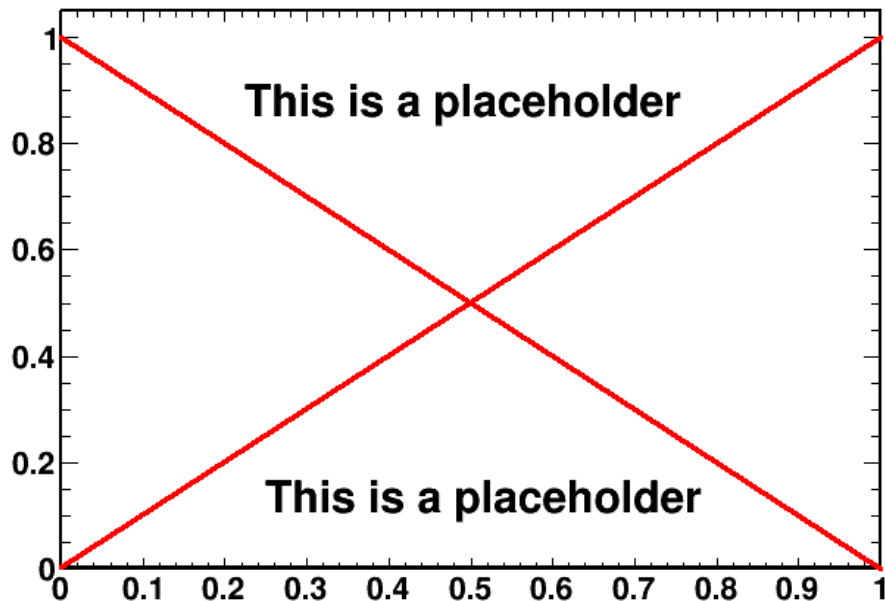


Figure 1.3.: chi2 distribution of first fits (not mines)

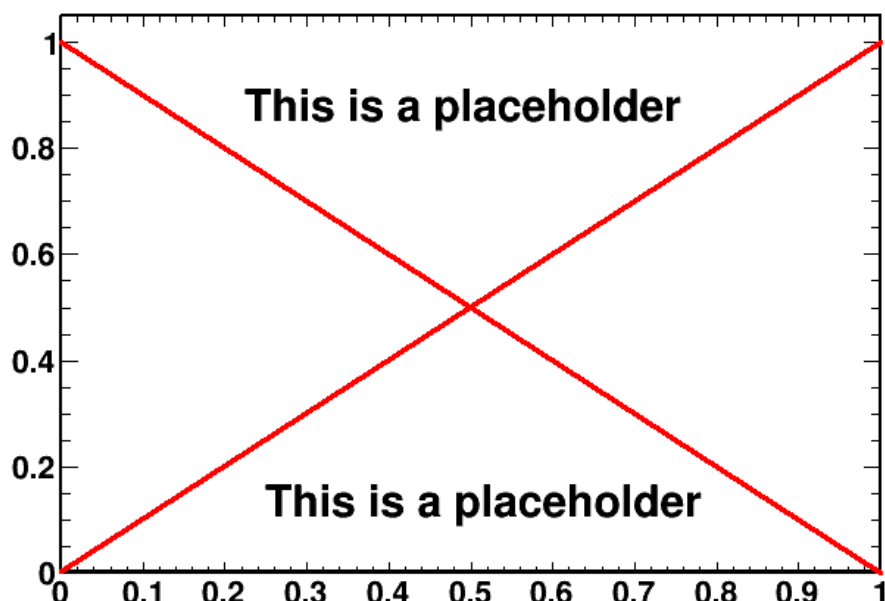


Figure 1.4.: shape of the excess

First is the presence of dark matter in the galaxy in the form of weakly interacting massive particles (WIMP). The spatial distribution of these particles would follow a Navarro-Frank-White (NFW) profile centered at the GC. They are also expected to produce gamma rays when annihilating with each other via hadrons production. In theory, if the mass of a WIMP particle is around 50GeV, the expected gamma spectrum would peak around 2GeV, where the excess is observed. (**cite**) The study of the excess could put strong limits on the mass and annihilation cross section of such WIMP and confirm, or infirm the theory.

**ToDo**

The second theory does not involve new physic, but inobserved milli-second pulsars. They would also be spherically distributed around the GC and their gamma spectrum peaks around 2GeV. A few thousands of them would be needed to recreate the intensity of excess. The main default of this explanation resides in the fact that we have observed only a few hundreds? at most. That would requires a very high concentration and a reason why we can not observe them more easily.

## 2. Method

### 2.1. Data origin

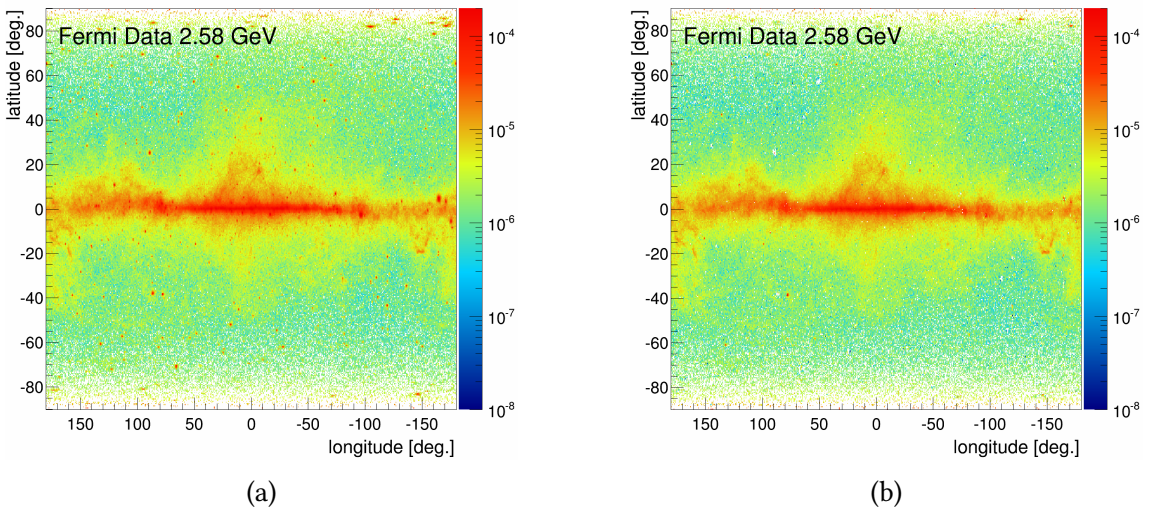


Figure 2.1.: Measured gamma ray flux before (left) and after (right) point source subtraction in  $\text{GeV}/\text{s}/\text{m}^2/\text{sr}$ . Most of the spots formed by point sources have disappeared, leaving only the diffuse background emission. The subtraction is not perfect, and can create artificial "holes" in the map (for example at coordinates (90, 25) or (50, 60)).

All the following work is based on the measurement of gamma rays coming from intra- and extra-galactic sources. The quality and accuracy of the data is one of the most important point that will determine the general quality of the results. Thus it is capital to be certain that the gathering and treatment was done properly.

The Fermi Large Area Telescope (LAT) observed the gamma-ray sky since 2008 and provides all the data of this work. All the information and data are available on the web and anybody can access them, using the tools given by Fermi.

Since the observation is still on-going it is important to stay up-to-date. The reconstruction method is also being improved regularly, improving every time the statistics, the systematic errors and the point source subtraction. One of the most important step in the treatment process is the first one, the selection of the events. Every photon measured is saved along with all its properties in a big data file. Then this long list is filtered to keep only the interesting observations. The filter can be based on the incoming direction, the energy or the time of observation, but also on the quality of the event reconstruction. This last cut can be critical. It will determine the chances that the measured event is in fact a gamma ray, and not some background noise polluting the data. Of course, the more strict the filter is, the less events are kept for analysis and the statistical errors can become large. This work uses the CLEAN class recommended by the Fermi team for diffuse emission analysis. ([cite Fermi sciencetools](#))

**ToDo**

The main parameters of the selection can be found in Tab 2.1.

Parameter name	Parameter value	Description
Event class	256 (CLEAN)	Quality parameter. Varies the level of background noise.
Event type	3	Back+front event.
Time boundaries	INDEF	Selecting all events since beginning of observation
Minimum energy (MeV)	58.4731	Minimum energy of the event.
Maximum energy (MeV)	513056	Maximum energy of the event.
zmax (degrees)	90	Maximum zenith angle to get rid of the Earth limb contaminations, as recommended by the LAT instrument team

Table 2.1.: List of the main parameters used for data selection.

An other important point is the creation of the exposure map. It basically tells how long the telescope spend observing a given part of the sky. After dividing the count map by the exposure, a flux map is obtained that does not depends on the observation time of particular regions.

The goal of this work is to study the diffuse sources of gamma-rays from inside and outside the milky way. Of course, the LAT does not differentiate them from point sources gamma rays. This has to be done manually as the last step in the treatment process. A large catalog of gamma ray point sources (3FGL) is available on line on NASA website ([cite site](#)). This catalog lists most of the known and identified point sources, along with their spectral shape and flux. This information can then be used to model the number of counts coming from point sources and their spatial and energetic distribution. To achieve this, the point sources properties must be combined with the instrument properties. For example, the point source flux is multiplied by the exposure time corresponding to its position. This flux must also pass through the instrument and its defaults will deform the initial shape of the source. For a point source, the final image obtain on the detector is the Point Spread Function (PSF) of the telescope and is given with the fermi tools. Every point source is convoluted by the PSF corresponding to the initial event selection, creating the final point source map as would be observed by the instrument. Once this model map is obtained, it is subtracted from the data to only keep the diffuse emission (see Fig. 2.1). Since the models are never perfect and all point sources are not listed, errors

**ToDo**

or anomalies in the observations can appear. Keeping the dataset up-to-date allows to use the latest catalogs and avoid a lot of mistakes.

Once all the treatment is done, a flux map of the entire sky in  $\text{counts}/\text{s}/m^2/\text{GeV}/\text{sr}$  is produced. The map is divided in bins of  $0.5 \times 0.5$  degrees on a Cartesian projection. Every bin contains 30 logarithmic energy bins ranging from 60 MeV to 513 GeV with a 1.2 multiplicative step. The final data cube is thus of dimension  $720 \times 360 \times 30$ . For visibility purposes, every energy bin is multiplied by its energy squared, becoming an energy flux in  $\text{GeV}/\text{s}/m^2/\text{sr}$ . This will be the default units used for the rest of this work.

The errors on the data are coming from two sources. First are systematic errors introduced by the instrument or the treatment process. They are around 3%, but can increase for low or high energies (Fig. 2.2). The second source is the statistical errors, proportional to the square root of counts. This property will make them decrease when the acquisition time will increase. They are dominant at high energy (above 50 GeV) where events are rare. On contrary at low energies (around 100 MeV), the systematic errors dominate. The final equation is the following :

$$\sigma_{tot} = \sqrt{\sigma_{sys}^2 + \sigma_{stat}^2} = \sqrt{\sigma_{sys}^2 + \frac{1}{N}} \quad (2.1)$$

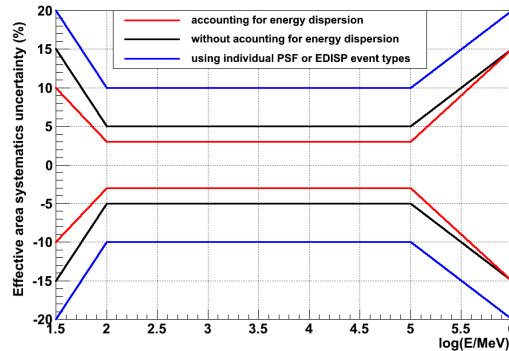


Figure 2.2.: Systematic error for Pass 8 data as function of the energy and the treatment quality. The energy dispersion is an effect of the uncertainty when measuring a photon's energy. Accounting for it when calculating the instrument response function can be critical at very low energies (around a few hundred MeV), where the statistical uncertainties are not dominant anymore.

## 2.2. Model components

### 2.2.1. Basic components

#### 2.2.1.1. $\pi^0$ production by propagated cosmic rays (PCR)

The initial propagated proton spectrum for the PCR template is obtained from the observed proton data from AMS-02 A good approximation is an unbroken power law ( $R-\alpha$ ) with a spectral index ( $\alpha$ ) of 2.85 at rigidities above 45 GV. At lower rigidities the data are below the power law because of solar modulation , as seen in Fig. 2.3a, where the AMS-02 data are plotted as well. To find the best parametrization, several indexes and breaks were tested. The optimal parametrization was found by interpolation between the fits

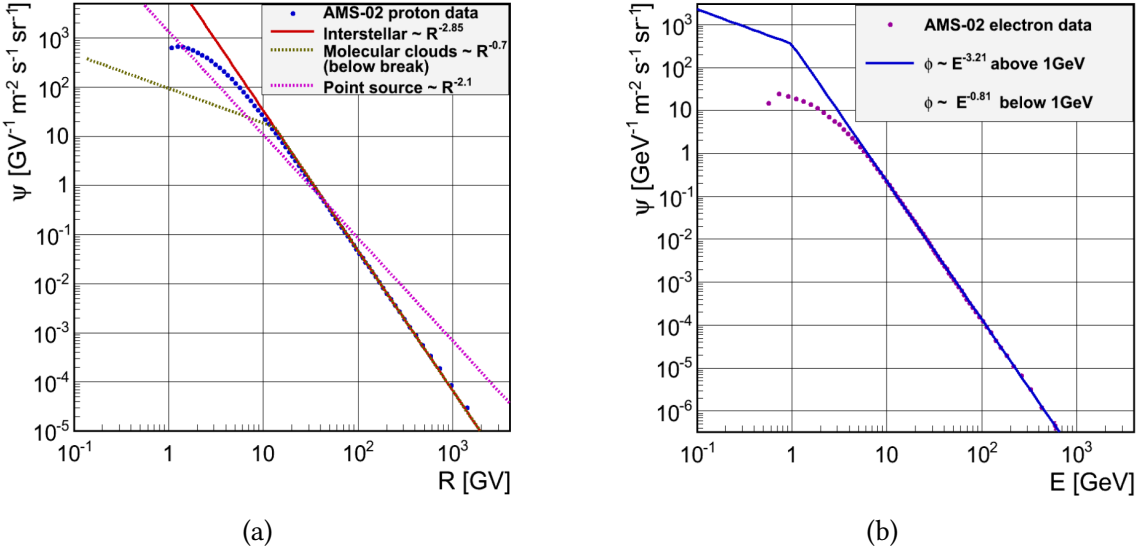


Figure 2.3.: Cosmic ray spectra used to determine the gamma ray templates. (a): Power-law proton spectra used to produce the PCR, MCR and SRC templates. In comparison, the measured data by AMS-02. (b): Power-law electron spectra used to produce the IC and BR templates, compared once again with AMS-02 data.

with the best test statistic. Finally, the gamma-ray data are well described by an unbroken power law for the protons with a spectral index ( $\alpha$ ) of 2.85 at all rigidities.

### 2.2.1.2. Inverse Compton (IC) and bremsstrahlung (BR)

The interstellar electron spectra needs a break around 0.2 GeV with a spectral index of 3.21 above. This is compatible with the locally observed electron spectrum (see Fig. 2.3b). Below the break the optimal spectral index is 0.81, which implies a suppression of electrons. The targets for the production of gamma-rays are the interstellar gas for BR and the interstellar radiation field (IRF) for IC, which are both strongly dependent of position, so the photon composition varies with sky direction. For this reason, we have to calculate the IC templates for each sky direction. The variation over the sky is about  $\pm 10\%$ , as shown in 2.4a. The BR template only depends on the interstellar gas distribution, decreasing the variations considerably compared to IC, as shown in 2.4b.

## 2.2.2. Additional components

### 2.2.2.1. $\pi^0$ production by source cosmic rays (SCR)

The proton spectra producing the SCR template can be described by a power law with a spectral index of 2.1, as obtained from the best gamma-ray template fit. The index 2.1 for the SCR template is expected from diffuse shock wave acceleration. The source cosmic rays are accelerated, or escape from the galaxy, hence a harder spectrum at high energies.

### 2.2.2.2. $\pi^0$ production by molecular clouds cosmic rays MCR)

A proton spectrum with broken power-law can parametrize the decreasing gamma-ray emissivity from MCs below 2 GeV. The break can vary from 6 to 14 GeV for different

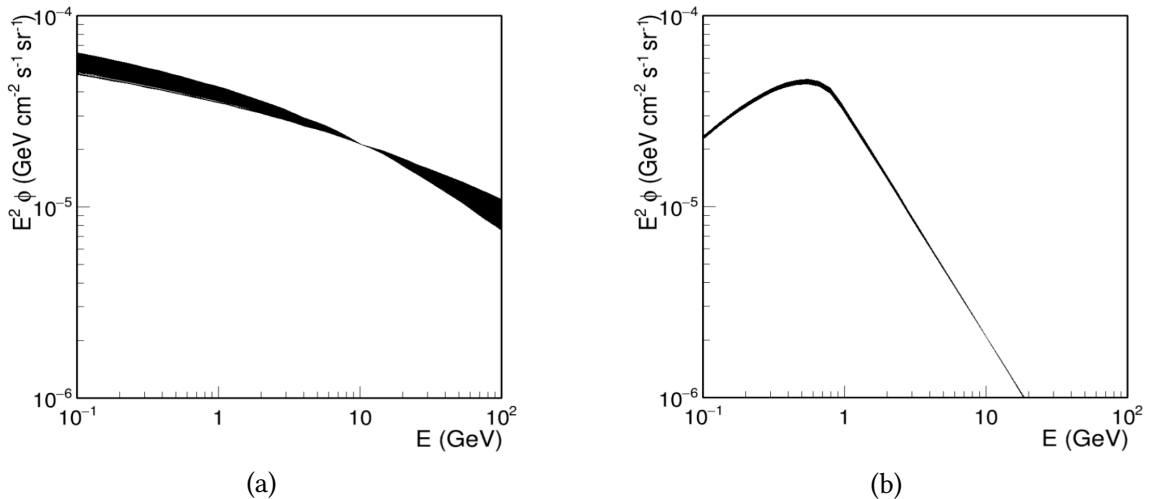


Figure 2.4.: (a): Superposition of the inverse Compton template in every sky direction, normalized at 10GeV. (b): Superposition of the bremsstrahlung template in every sky direction, normalized at 10GeV.

clouds according to the fit. Above the break an optimal spectral index of 2.85 was found to be the same as for the PCR spectrum, as expected if the high energy propagated protons are above a certain magnetic cutoff. Below the break, the spectral index is 0.7, thus providing a significant suppression of protons below the break, as can be seen from Fig. 2.3a. This lower break spectral index does not have a strong influence on the fit and therefore was taken to be 0.7 GeV. Variations in the magnetic cutoff in MCs are expected from the variations in size and in magnetic field, the latter increasing with MC density. These variations between 6 and 14 GeV varies the maximum of the gamma-ray spectrum around a few GeV.

### 2.2.2.3. Dark matter annihilation (DM)

Dark matter particles are expected to annihilate and produce hadrons of roughly twice the WIMP mass, just like in electron-positron annihilation. This should produce copious amounts of gamma-rays from  $\pi^0$  decays. A smaller fraction of WIMP annihilation can lead to tau lepton pairs, which can lead to  $\pi^0$  production in the hadronic tau decays. This contribution is expected to be small and is neglected. The DM template can be calculated with the DarkSusy software. ([cite\[67, 68\]](#)) An annihilation signal peaking around 2-3 GeV requires a WIMP mass around 50 GeV, as shown in Fig. 2.5a. The DM template falls down to zero for energies above twice the WIMP mass, which differentiate it from the MCR spectrum with a much softer spectrum.

ToDo

### 2.2.2.4. Milli-second pulsars gamma-ray production (MSP)

The MSP template is directly taken from the Fermi study . They simulated the emission of 1700 milli-second pulsars with different energies around the galactic center. The high energy shape of the spectrum resemble closely the DM template, but the main difference with DM and MCR is for low energies. Indeed, below 1 GeV, the MSP template is a lot softer and this feature makes it discernible from the two others.

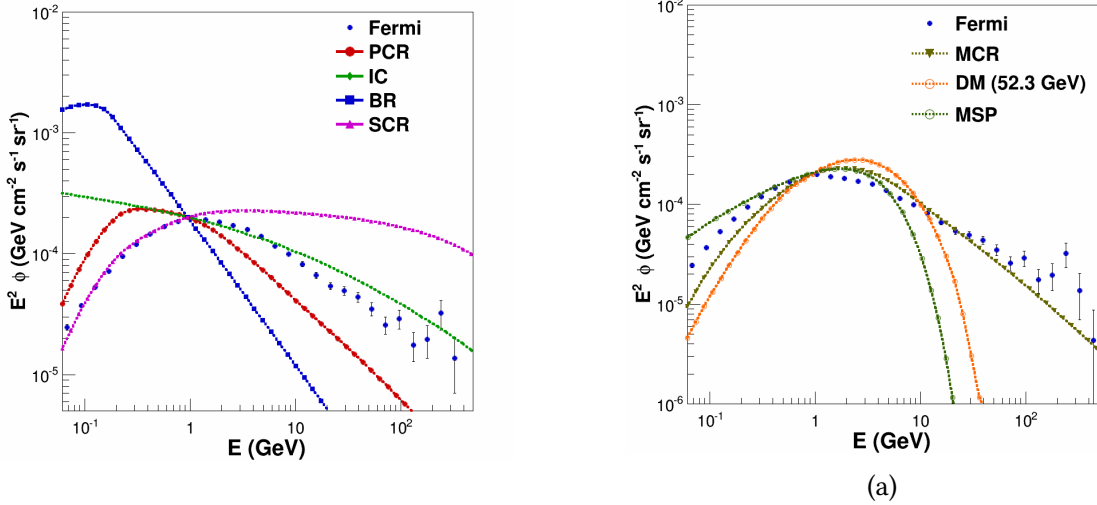


Figure 2.5.: (a): Comparison of PCR, IC, BR and SCR templates, normalized at 1 GeV. Measured data from the central molecular zone is shown as well. (b): Comparison of the three excess components, along with the data from the CMZ.

### 2.2.2.5. Isotropic component

The isotropic template represents the contribution from the isotropic extragalactic background and hadron mis-identification. Its spectral shape and absolute normalization are provided within the Fermi software ([cite\[51\]](#)), but it was redetermined for the analysis as follow. A first fit of the data in regions outside the Bubbles and the Galactic disk using the isotropic template from the Fermi software is produced as an initial estimate. If one plots the total observed gamma-ray flux versus the fitted flux in the various cones in a certain energy bin, one expects a linear relation crossing the origin if the isotropic flux is estimated correctly (See Fig. 2.6). However, if the isotropic contribution is either too low or too high, an offset at the origin is introduced in the linear relation. Since the isotropic component is by definition the same for all cones for a given energy, this offset can be subtracted from the Fermi template to improve the fit. Once the offset is determined for each energy bin and subtracted from the original template, the process is repeated until the offset converges to zero.

**To Do**

## 2.3. Fitting method

The fitted data can be seen as a data cube whose dimension are longitude, latitude and energy. The finest spatial grid is divided in  $720 \times 360$  cones of  $0.5^\circ \times 0.5^\circ$ . Every cone contains 30 energy bins. This allows to treat different portions of the sky independently of one another. Since the cones do not have the same solid angle and the statistic in a small binning can be problematic, the grid is more often composed of 797 bins of different sizes, bigger at the poles and smaller near the equator. This allows a better statistic in lower flux regions and where a high spatial resolution is not needed (i.e. at high latitudes). In the same time, the equator and the GC have a lot more counts and can be treated in a smaller binning. This binning is faster to compute than a regular grid with an good enough output quality to study the results.

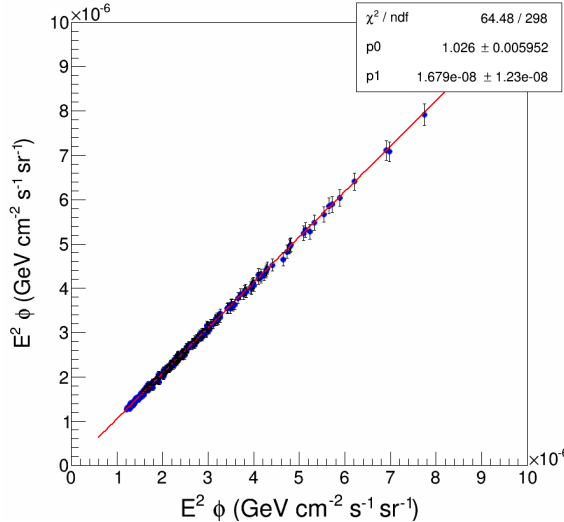


Figure 2.6.: The fitted data (abscissa) versus the observed data (ordinate) in every region of the sky for a given energy of 1 GeV. A linear fit is performed to find the offset at the vertical axis. This number represent the amount the isotropic component shifts the data in all cones. Once this is done for every energy bin, the offset is added to the previous isotropic template and the process is repeated until convergence.

The fit uses a certain number of components (three at least) each corresponding to a certain phenomenon and described earlier. They all have a certain energy spectra, that can vary with the position in the sky in the case of IC (See Fig. 2.5).

The fits are done for every bin independently. After choosing the templates used for the fit, their scaling factor is the only degree of freedom allowed. Using a ROOT TVirtualFitter object, every template is scaled up or down until their sum comes the closest to the data. Mathematically, the minimum distance between the model and the data is found when the  $\chi^2$  value is lowest. It is calculated as follows:

$$\chi^2 = \sum_{i=1}^{30} \left[ \frac{\left( D_i - \sum_{j=1}^n [n_j \cdot T_{ij}]^2 \right) + iso}{\sigma_i^2} \right]^2 \quad (2.2)$$

where:

- $D_i$  is the data flux in the  $i^t h$  energy bin.
- $n_j$  is the scaling factor for the  $j^t h$  model component.
- $T_{ij}$  is the model flux of the  $j^t h$  in the  $i^t h$  energy bin.
- $\sigma_i$  is the geometric mean of the statistical and systematical error of the Fermi data point  $i$ .

The fit is very well constrained with only five or six degrees of freedoms depending on the model against 30 data points. A useful value is the  $\chi^2/d.o.f$  where  $d.o.f = \#data\ points - \#degrees\ of\ freedom - 1$ . This rescaling has the advantage to bring the perfect  $\chi^2$  value down to one, thus making the comparison between different fits

easier. This rescaling will be applied every time when speaking about  $\chi^2$  in the rest of the discussion, except if explicitly told. The closest a  $\chi^2$  value is to one, the better the model follows the data. The higher it gets, the lower the quality of the fit. It can also happen that it gets lower than one. This can happen when the fit is good, but the error bars on the data are too big.

Since every bin is fitted independently, it is not possible to implement a spatial template, i.e. where the spatial shape of a component would be fixed in advance. For example a component with a spherical distribution around the GC, as can be done in other works (**cite**). The hope is to let the fit find reasonable shapes by itself only using the  $\chi^2$  minimization technique.

This fitting method offers many ways to look at the results, depending on the interest. It is possible to produce flux maps of each component to study their spatial shapes at different energies. This can for example show a correlation between a certain template and a galactic feature such as the disk or the bubbles. An other way is to create a spectrum of one cone to look at the relative quantity of every template at different energies. This can put into evidence problems in the models and help perfect the spectral shape of the components.

The first step when testing a new model is to see if it can reproduce results of previous studies. Only once it works and can be confidently used can it produce new results.

**ToDo**

## 3. Results

### 3.1. Recreating previous results

Introduce the weniger plots here (or in the state of the research?) to show excess in GC.

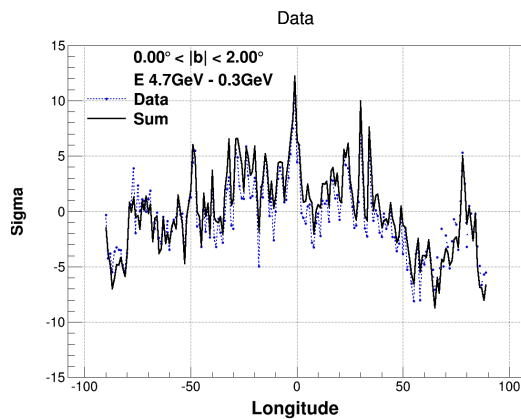


Figure 3.1.: Some weniger plots to show the GC excess

Before trying upgrade the model in use, it is important to make sure we can recreate it with the same parameters. Fig. 3.2 shows the results of a fit using only the PCR, IC and BR components. The shape and intensity of the previously observed excess are found ([cite](#)). ToDo

It can also be observed that the fit is particularly bad in the bubbles and the disk (see Fig. 3.2) where the high energy spectrum is harder (see Fig. 3.3). In this region, the PCR spectrum falls off too quickly, and the IC spectrum which usually takes care of high energies is blocked by the low energy flux drop.

### 3.2. Introducing SCR

Introducing the SCR template, a clear improvement can be noted in the  $\chi^2$  distribution (see Fig. 3.4). The bubble shape that was clear before has now disappeared. Even if the fit is still not perfect everywhere, the improvement is significant.

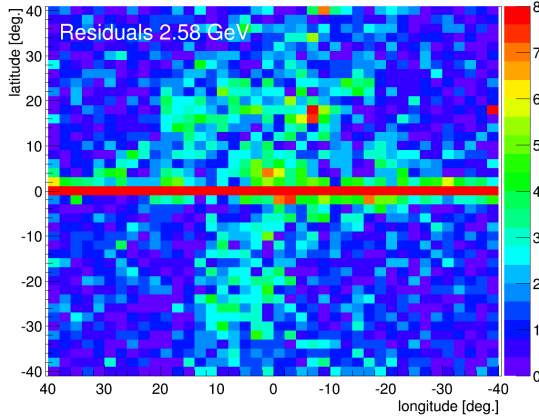


Figure 3.2.: Picture of GC excess, (compare with previous papers?), a chi2 map too

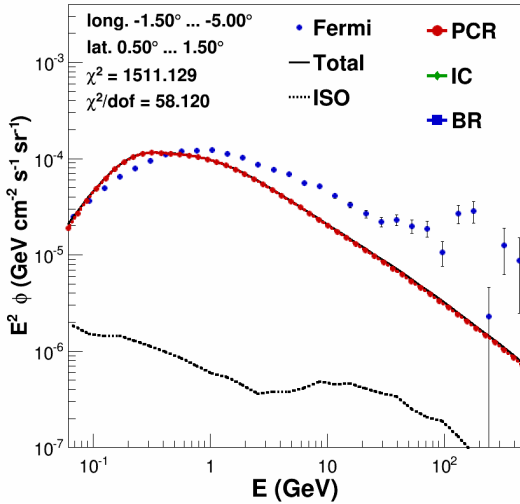


Figure 3.3.: Picture background only spectra with bad fit (high energies too hard) Compare bubble or disk region and outside

From Fig. 3.5a and 3.5a we see the role of the SCR template at high energies, taking care of the high flux. It also permits a better fit of low energies by PCR and IC since they do not have to be everywhere at the same time.

**ToDo**

(**Here the bad chi2 comes from 0.1GeV region, where the PCR template does not fit the data. not from the 2GeV excess.**) A problem still remains in the disk and diffuse regions around the galactic anticenter.

### 3.3. Introducing SCR and MCR

As shown on Fig. 3.6, the addition of a new template improve significantly the  $\chi^2$  distribution in all directions. The bubbles and the disk structures are not visible anymore.

Three dots appear to have a really high  $\chi^2$ , but that is only due to the point source subtraction that is not perfect (see Chapt. 2.1).

Fig. ?? shows the central molecular zone (CMZ) fitted with and without the MCR component. The gas density is very high in this region, hence it is the first region where we

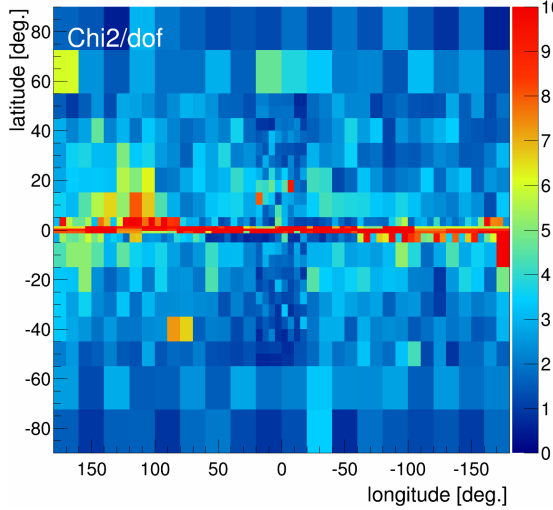
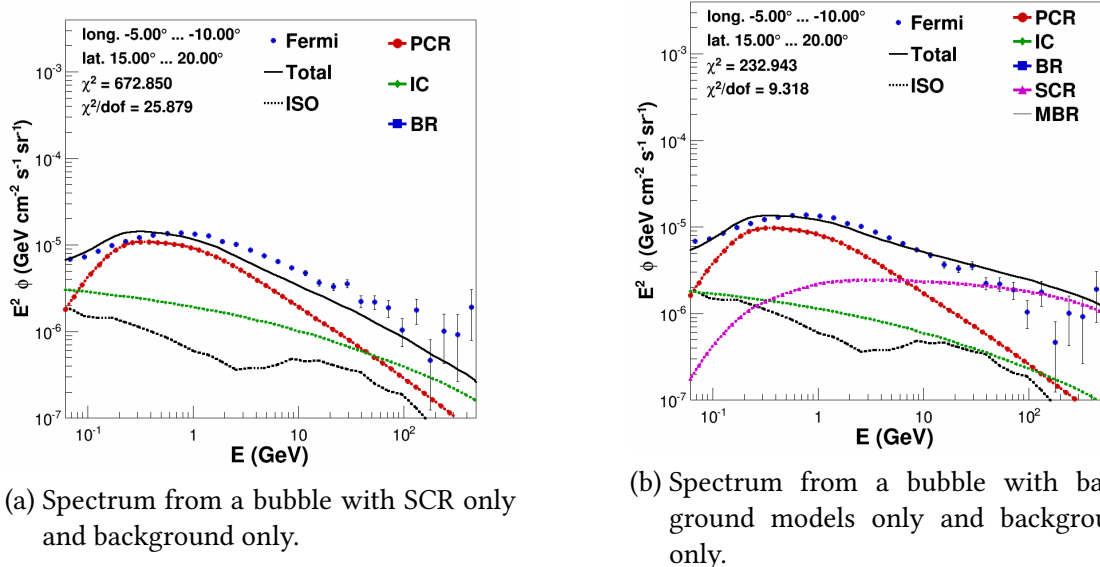


Figure 3.4.: Chi2 distribution of SCR only fits.



(a) Spectrum from a bubble with SCR only and background only.

(b) Spectrum from a bubble with background models only and background only.

would expect the MCR emission to be present, if not dominant compared to PCR. Indeed the fit chooses this configuration, with the MCR template dominating all the others and we can directly see the improvement in the MCR fit. The energies around 2GeV had a clear excess that the four components of the SCR fit could not account for. The MCR template peaking in this region, it comes in very handy and fill this gap, Leaving the SCR template taking care of the high energies and PCR and BR for the low energies. **(Why To Do isn't there IC? -> Wait to see if we change the models)**

### 3.3.1. Discussion on spatial shapes

Fig. ?? shows the spatial distribution of the flux of each component around 2GeV, as returned by the fit.

The bremmstrahlung component is consistent with the the expectations. Present everywhere, it is strong in the disk, and decrease a little in the bubbles.

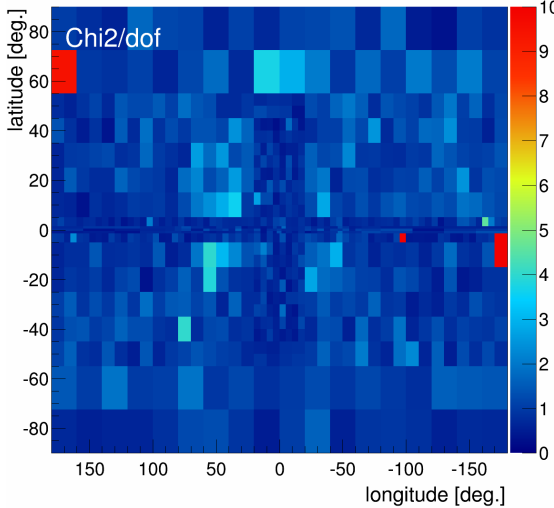
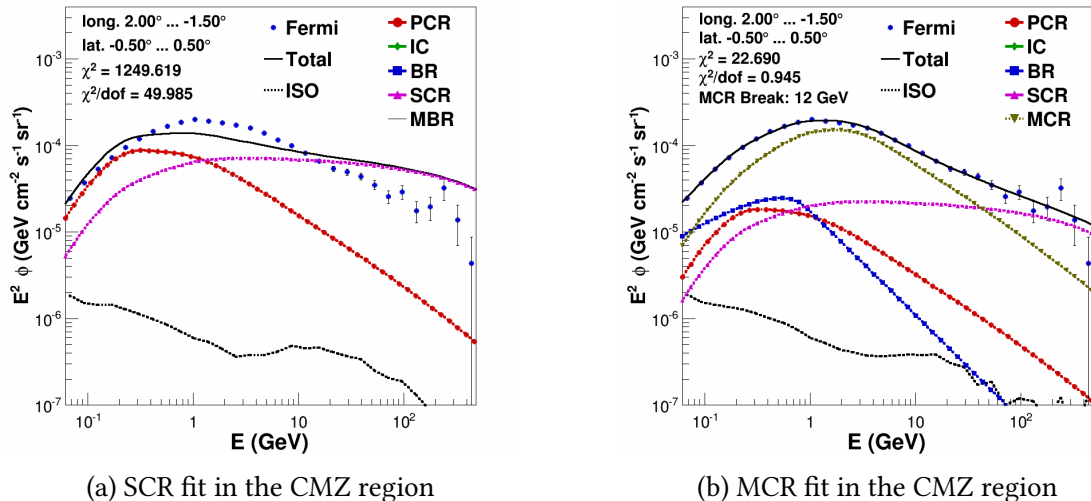


Figure 3.6.: Chi2 maps of MCRonly fits compared to background only



Though the general shape is spherical, the IC component has an unexpected feature in the form of a strong depletion in the disk, like a "sandwich" structure. This is surprising in the sense that this is where the interstellar radiation field (ISRF) and electron density are supposed to be maximal, creating a higher IC flux. A possible explanation could be coming from the dust distribution, screening the starlight component of the ISRF. Thus depriving the ISRF of its main component and leaving only the dust infra red emission and the CMB to interact with the electrons. This could result in a lower IC gamma-ray flux in the disk.

The SCR component is playing his role perfectly, filling the bubbles and the disk, where the high energy portion of the spectra needs a harder spectrum. It traces perfectly the sources distribution in the disk and the outflow of high energy protons in the bubbles.

The general shape of PCR looks coherent with the shape of the galaxy, with a strong flux in the bar and the galactic disk in general. When looking closely, one can see the same kind of depletion in the disk than for IC, even if the effect is less remarkable. This finds its cause in the MCR distribution with a very high flux in the disk. The sum of both

templates (MCR + PCR) shows no sign of such a feature, which tends to show that some of the PCR photons are absorbed by the MCR template. But the total is coherent, with no unexplainable central gap.

The MCR template also follows the spatial distribution of molecular clouds in our galaxy. It is a good sign since it is supposed to come from those regions. It is not spherical at all. That could have happened if the excess component has a DM origin, since it is supposed to be spherically distributed.

### 3.4. Introducing SCR and DM

The first step is to determine which mass for the WIMP particles would produce the best spectrum for our fit. Fig. 3.9 shows the best fit for the CMZ region, with the WIMP mass as a free parameter. It chooses a mass of 52.3 GeV, peaking around a few GeV, as expected in (ref theory section). Since the excess is the most significant in this region, it is also the best place to define our mass for the rest of the sky. This is what is done in the following section.

**ToDo**

Once the mass is determined for the entire sky, the fit gives the following results. The  $\chi^2$  distribution (Fig. 3.10 is comparable to the MCR fit for the major part but is significantly worst in the disk.

As seen on Fig. 3.11, the DM distribution of the fit traces closely the distribution of molecular gas distribution (as traced by CO).

### 3.5. Introducing SCR and MSP

The first thing that can be noticed when seeing the  $\chi^2$  distribution of the MSP only fit (Fig 3.12) is the similitudes with the DM only fit (Fig. 3.10). The fit succeeds pretty well outside the disk, but gets significantly worst when  $|b| < 2$ .

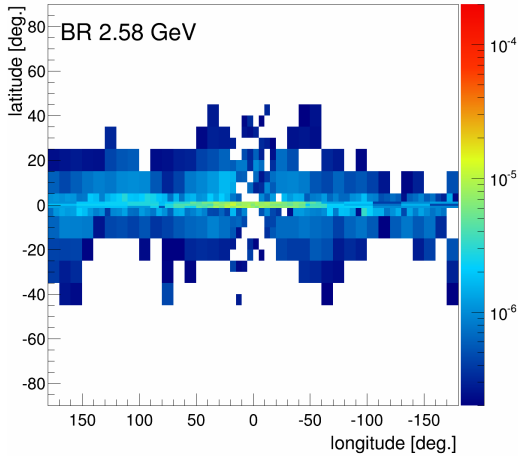
Using the MSP spectrum predicted by fermi (cite) to fit the CMZ region does not give entire satisfaction. The CMZ is in the disk, where the  $\chi^2$  is generally worst.

**ToDo**

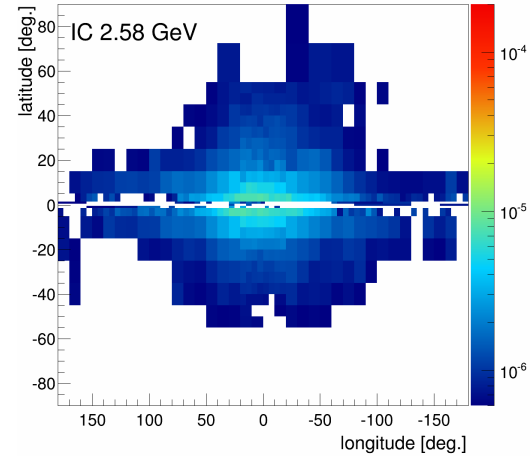
The distribution of MSP in the sky ressembles the distribution of MCR and DM obtained in previous sections. Present everywhere in the disk, with a higher flux in GC and the bubbles.

(add picture of residuals at low energy maybe?)

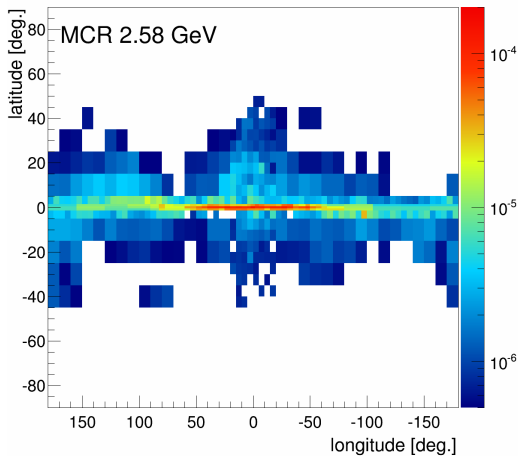
**ToDo**



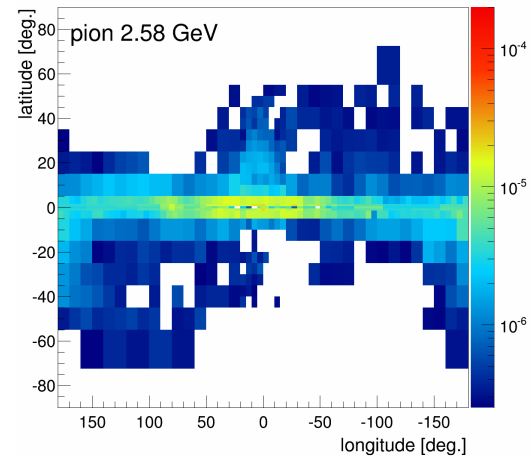
(a) Flux distribution of bremstrahlung (BR)



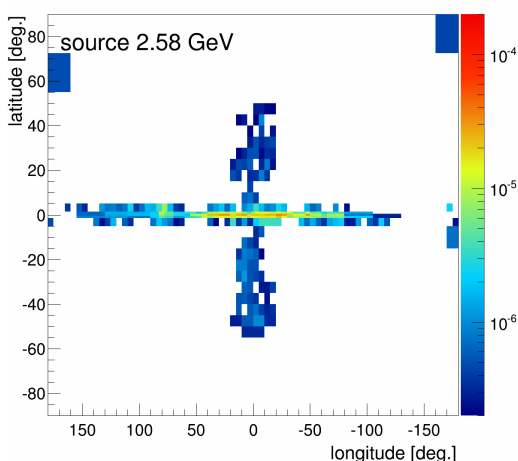
(b) Flux distribution of inverse compton (IC)



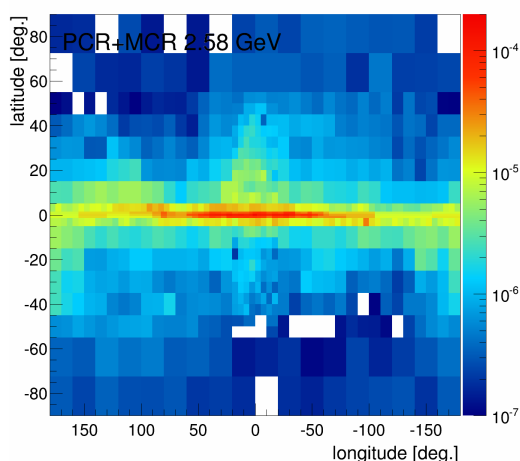
(c) Flux distribution of MCR



(d) Flux distribution of PCR



(e) Flux distribution of SCR



(f) Flux distribution of PCR + MCR

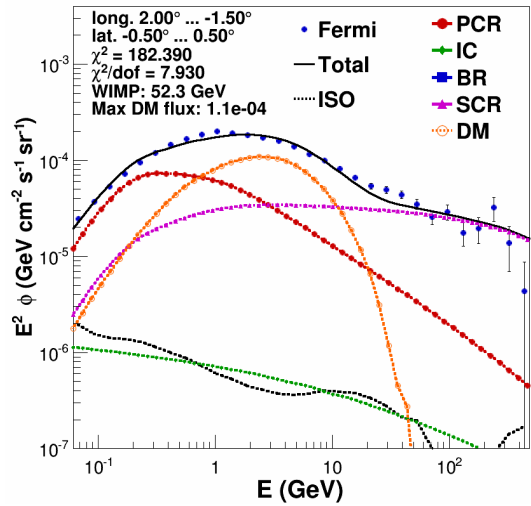


Figure 3.9.: spectrum of best mass DM fitted in CMZ. Also pictures of DM distribution compared to gas map.

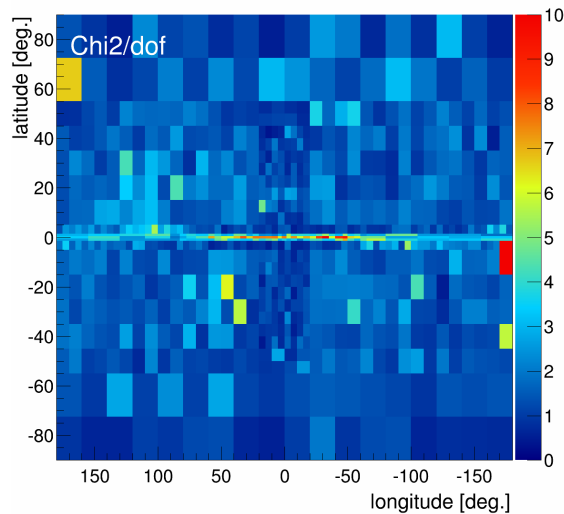


Figure 3.10.: DM fit chi2 distribution

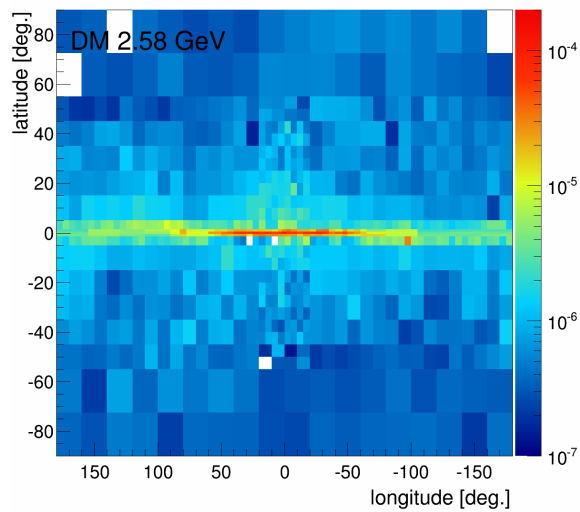


Figure 3.11.: DM distribution compared to gas map.

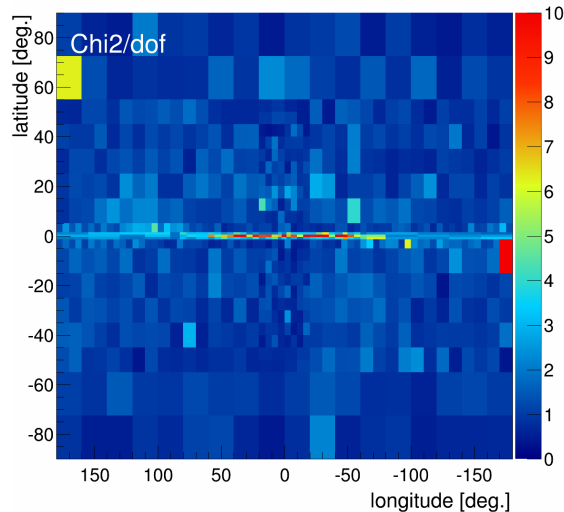


Figure 3.12.: Chi2 distribution of MSP only fit

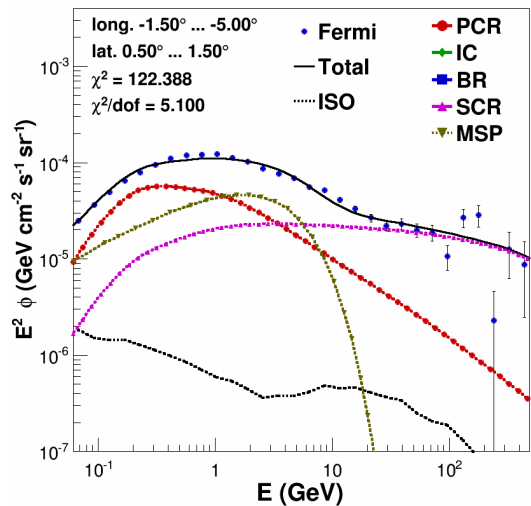


Figure 3.13.: Fit with SCR and MSP spectrum in the CMZ region.

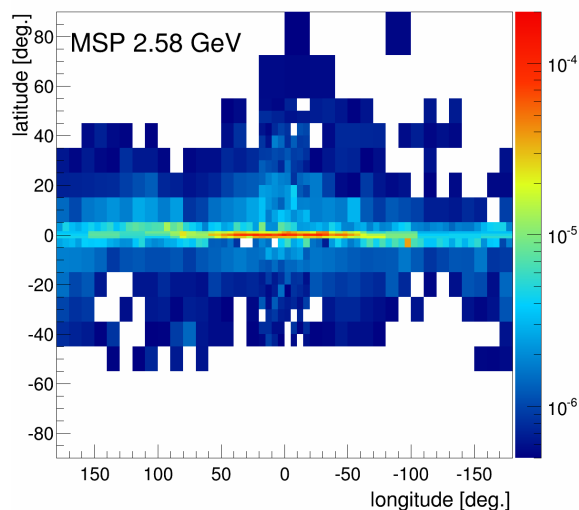


Figure 3.14.: Flux distribution of MSP around 2.5GeV.



## **4. Discussion**

### **4.1. Interpretation of spatial shapes**

### **4.2. Why is MCR better than DM or MSP**

Gathering the results of the previous section, a conclusion tends to emerge : the fit clearly prefers the MCR hypothesis over DM and MSP. We will discuss why in this section.

First of all, comparing the  $\chi^2$  skymaps is pretty clear. Adding a fifth component over SCR is an improvement in all cases, but the best fits are obtained with MCR, especially in the disk.

### **4.3. How do these results fit in context**



## **5. Conclusion**

Here you write some Conclusion.



# Bibliography

- [1] Aguilar, M. et al., *Phys. Rev. Lett.* **2013**, *110*, 141102.
- [2] Vagelli, V. Measurement of the cosmic  $e^+ + e^-$  Flux from 0.5 GeV to 1 TeV with the Alpha Magnetic Spectrometer (AMS-02) on the International Space Station. Ph.D. thesis, Karlsruher Institut für Technologie (KIT), 2014.
- [3] BibTeX on Wikipedia, <https://en.wikipedia.org/wiki/BibTeX>, Version Date: 2017-09-19.



# List of Figures

1.1.	The Milky Way, as seen from two different angles. . . . .	3
1.2.	Orbital velocity of the Milky Way as a function of the radius. A clear discrepancy between the theory and the observation can be seen above a 2 kpc radius. Source: Matthew Newby, Milkyway@home . . . . .	4
1.3.	chi2 distribution of first fits (not mines) . . . . .	7
1.4.	shape of the excess . . . . .	7
2.1.	Measured gamma ray flux before (left) and after (right) point source subtraction in $GeV/s/m^2/sr$ . Most of the spots formed by point sources have disappeared, leaving only the diffuse background emission. The subtraction is not perfect, and can create artificial "holes" in the map (for example at coordinates (90, 25) or (50, 60)). . . . .	9
2.2.	Systematic error for Pass 8 data as function of the energy and the treatment quality. The energy dispersion is an effect of the uncertainty when measuring a photon's energy. Accounting for it when calculating the instrument response function can be critical at very low energies (around a few hundred MeV), where the statistical uncertainties are not dominant anymore. . . . .	11
2.3.	Cosmic ray spectra used to determine the gamma ray templates. (a): Power-law proton spectra used to produce the PCR, MCR and SRC templates. In comparison, the measured data by AMS-02. (b): Power-law electron spectra used to produce the IC and BR templates, compared once again with AMS-02 data. . . . .	12
2.4.	(a): Superposition of the inverse Compton template in every sky direction, normalized at 10GeV. (b): Superposition of the bremsstrahlung template in every sky direction, normalized at 10GeV. . . . .	13
2.5.	(a): Comparison of PCR, IC, BR and SCR templates, normalized at 1 GeV. Measured data from the central molecular zone is shown as well. (b): Comparison of the three excess components, along with the data from the CMZ. . . . .	14
2.6.	The fitted data (abscissa) versus the observed data (ordinate) in every region of the sky for a given energy of 1 GeV. A linear fit is performed to find the offset at the vertical axis. This number represent the amount the isotropic component shifts the data in all cones. Once this is done for every energy bin, the offset is added to the previous isotropic template and the process is repeated until convergence. . . . .	15
3.1.	Some weniger plots to show the GC excess . . . . .	17
3.2.	Picture of GC excess, (compare with previous papers?), a chi2 map too . .	18

3.3.	Picture background only spectra with bad fit (high energies too hard) Compare bubble or disk region and outside . . . . .	18
3.4.	Chi2 distribution of SCR only fits. . . . .	19
3.6.	Chi2 maps of MCRonly fits compared to background only . . . . .	20
3.9.	spectrum of best mass DM fitted in CMZ. Also pictures of DM distribution compared to gas map. . . . .	23
3.10.	DM fit chi2 distribution . . . . .	23
3.11.	DM distribution compared to gas map. . . . .	24
3.12.	Chi2 distribution of MSP only fit . . . . .	24
3.13.	Fit with SCR and MSP spectrum in the CMZ region. . . . .	25
3.14.	Flux distribution of MSP around 2.5GeV. . . . .	25

# **Appendix**

## **A. Some appendix section**

This appendix chapter contains ...

